ACS APPLIED MATERIALS & INTERFACES

Research Article

www.acsami.org

Facile Route to the Controlled Synthesis of Tetragonal and Orthorhombic SnO_2 Films by Mist Chemical Vapor Deposition

Jae-Yoon Bae,[†,‡] Jozeph Park,[§,‡] Hyun You Kim,[*,⊥] Hyun-Suk Kim,[*,⊥] and Jin-Seong Park[*,†]

[†]Division of Materials Science and Engineering, Hanyang University, 222 Wangsimni-ro, Seoul 133-719, Republic of Korea

[§]Department of Material Science and Engineering, Korea Advanced Institute of Science and Technology, Daejeon 305-338, Republic of Korea

[⊥]Department of Materials Science and Engineering, Chungnam National University, Daejeon 305-764, Republic of Korea

Supporting Information

ABSTRACT: Two types of tin dioxide (SnO_2) films were grown by mist chemical vapor deposition (Mist-CVD), and their electrical properties were studied. A tetragonal phase is obtained when methanol is used as the solvent, while an orthorhombic structure is formed with acetone. The two phases of SnO_2 exhibit different electrical properties. Tetragonal SnO_2 behaves as a semiconductor, and thin-film transistors (TFTs) incorporating this material as the active layer exhibit n-type characteristics with typical field-effect mobility (μ_{FE}) values of approximately 3−4 $cm^2/(V\ s)$. On the other hand, orthorhombic SnO_2 is found to behave as a metal-like transparent conductive oxide. Density functional theory calculations reveal that orthorhombic SnO_2 is more stable under oxygen-rich conditions, which correlates well with the experimentally observed solvent effects. The present study paves the way for the controlled synthesis of functional materials by atmospheric pressure growth techniques.

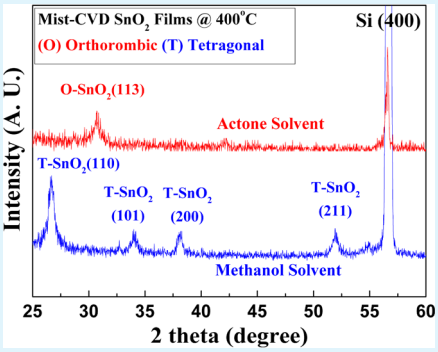

KEYWORDS: *tin dioxide, mist chemical vapor deposition, thin-film transistors, field-effect mobility, active layer, density functional theory*

INTRODUCTION

Tin dioxide (SnO_2) is a widely used material for applications such as transparent electrodes,[1] semiconductors,[2] solar cells, and gas sensors.[3−10] SnO_2 may exhibit two different crystalline phases: either a tetragonal (rutile) or an orthorhombic structure.[11] Most reports have been focusing on the naturally occurring tetragonal phase, for applications including gas sensors and n-type semiconductors.[2,9,10] On the other hand, orthorhombic SnO_2 is more difficult to fabricate because it is stable at relatively high pressure and temperature conditions.[12,13] Because this material may exhibit distinct electrical properties with respect to its crystal structure, which involves a relationship that has not been systematically studied yet, it is anticipated that the ability to control the SnO_2 microstructure may provide a broad range of applications and, hence, a more effective use of this versatile solid.

A few research groups have successfully produced orthorhombic SnO_2 thin films utilizing vacuum deposition techniques at moderately low pressures and temperatures.[14−16] However, such vacuum-based processes are expensive, being a major obstacle for the realization of low-cost, large-area electronics. In this regard, solution-based processes have attracted great attention as cost-effective film growth methods because they do not necessitate vacuum atmospheres. It is well-known that the solvents used in the solution process play a critical role among several other variables. Many studies have reported on the effects of the solvent properties during the synthesis of organic and inorganic materials. For example, Chang et al. found that the boiling point and solubility of the solvent affect the performance of the resulting organic thin-film transistors (TFTs) to a significant extent.[17] Edusi et al. also observed during the growth of titanium dioxide (TiO_2) that the use of methanol-based solvents results in films with the rutile structure and that ethanol solutions favor the formation of anatase.[18]

In the present work, SnO_2 thin films are synthesized using mist chemical vapor deposition (Mist-CVD). The latter is a solution-based film growth technique that can be performed under atmospheric pressure with a simple, less expensive configuration.[19,20] It is observed that the use of different solvents in the precursor solution greatly affects the resulting crystalline phase of SnO_2. The different microstructures then induce distinct physical, optical, and electrical properties of the SnO_2 films. Typical n-type semiconducting characteristics are observed in TFTs incorporating tetragonal SnO_2 as the active layer, while devices fabricated with orthorhombic SnO_2 exhibit simple conductorlike behavior.

Received: March 14, 2015
Accepted: May 18, 2015
Published: May 18, 2015

DOI: 10.1021/acsami.5b02251
ACS Appl. Mater. Interfaces 2015, 7, 12074−12079

EXPERIMENTAL SECTION

The SnO_2 films were grown by Mist-CVD onto silicon substrates. Liquid solutions were prepared by dissolving tin(II) chloride dihydrate ($SnCl_2 \cdot 2H_2O$, Aldrich) in two different solvents, acetone and methanol, each to a concentration of 0.015 M. The two solutions were each stirred for 1 h on a hot plate at a temperature of 60 °C. Mist-CVD was processed with the following steps. The mist of the liquid source was generated by an ultrasonic atomizer (frequency: 1.5 MHz) and then carried into the chamber by the infiltration of N_2 carrier gas (5000 sccm). The mist was next vaporized within the chamber and deposited on the substrate under ambient atmosphere. The chamber was designed to form a laminar flow. The substrate temperature was varied between 250 and 400 °C. The entire process was carried out at a pressure of 1 atm. The film growth rate increases with increasing substrate temperature, suggesting a reaction-limited growth process (Figure S1 in the SI). The thicknesses of the SnO_2 films grown for TFT fabrication and film analyses were approximately 20 and 40 nm, respectively.

The microstructures and chemical states of the SnO_2 films were analyzed by X-ray diffraction (XRD) and X-ray photoelectron spectroscopy (XPS), respectively. In order to examine the electronic configuration near the conduction band, X-ray absorption near-edge structure (XANES) analyses were performed using a total electron yield mode at the BL-10D beamline of the Pohang Accelerator Laboratory, Gyeongsangbuk-do, Korea. The optical properties of the films were measured using an ultraviolet−visible (UV−vis) spectrophotometer and a spectroscopic ellipsometer. Height profile images of the film surfaces were obtained by atomic force microscopy (AFM).

For the fabrication of TFT devices, highly doped silicon substrates were used as gate electrodes, and thermally oxidized SiO_2 (100 nm) films were used as gate insulators. After the SnO_2 films were grown by Mist-CVD, indium−tin oxide (ITO) layers were sputter-deposited at room temperature to form the source/drain electrodes. The electrical properties of the TFT devices were analyzed using an HP 4155A semiconductor parameter analyzer in a dark room under ambient conditions. The channel width and length of each TFT device were 800 and 200 μm, respectively.

COMPUTATIONAL DETAILS

DFT calculations were performed in a plane-wave basis using the *VASP* code.[21] Because both the plane generalized gradient approximation (GGA)-level DFT calculations and the GGA+*U* formalism with a *U* value fitted to the formation enthalpy of SnO_2 cannot correctly describe the experimentally reported band gap of SnO_2 (tetragonal SnO_2: 3.60 eV),[22,23] the hybrid functional was implemented to describe the exchange-correlation energy.

SnO_2 phases were modeled using orthorhombic (ICSD 62199) and tetragonal (ICSD 84576) SnO_2 unit cells, with 4 × 4 × 6 (orthorhombic) and 6 × 6 × 4 (tetragonal) *k*-point grid samplings of the Brillouin zone. The final convergence criteria for the electronic wave function and geometry were 10^{-4} eV and 0.01 eV/Å, respectively. Valence electrons were described by plane waves up to an energy cutoff of 400 eV, and the core electrons were described within the projector augmented-wave framework.[24] The PBE0 hybrid functional was applied[25,26] to calculate the formation of the different SnO_2 phases. The resulting band-gap energy of tetragonal SnO_2 (3.54 eV) correlates well with the experimental value (3.60 eV).[22,23]

To investigate the mechanism of the solvent-selective occurrence of the SnO_2 phases, the free energies of formation for both SnO_2 phases were calculated as functions of the chemical potentials of oxygen and tin [see the Supporting Information (SI) for details].[27] The reference energy point for calculation of the chemical potentials of tin and oxygen was set to that of bulk β-Sn metal and the gas-phase O_2 molecule, respectively. The energetics of the solvent reduction by H_2 was calculated with the B3LYP functional[28,29] to compare the oxidizing power (the ability to supply oxygen) of methanol and acetone. The solvent molecules were reduced by H_2 to produce a corresponding alkane and water as follows:

$$CH_3OH + H_2 \rightarrow CH_4 + H_2O \qquad \Delta E_{red} = -1.366 \text{ eV}$$

$$C_3H_6O + 2H_2 \rightarrow C_3H_8 + H_2O \qquad \Delta E_{red} = -1.754 \text{ eV}$$

RESULTS AND DISCUSSION

Microstructural analyses of the SnO_2 films were performed by XRD, as shown in Figure 1. Films grown using the methanol

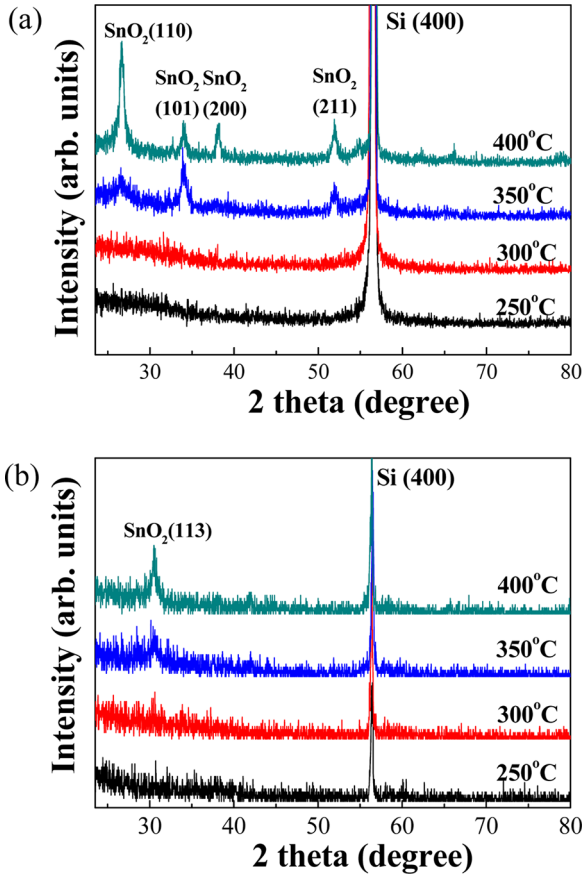

Figure 1. XRD patterns of SnO_2 films grown on silicon at different substrate temperatures using (a) methanol and (b) acetone solvents, resulting in (a) tetragonal and (b) orthorhombic crystals at elevated temperatures.

solvent exhibit a tetragonal phase of SnO_2 at substrate temperatures above 350 °C (Figure 1a), while those deposited using the acetone solvent appear to undergo crystallization at substrate temperatures above 300 °C (Figure 1b) but into an orthorhombic phase. AFM studies indicate that significant changes in the film roughness occur at substrate temperatures above 350 °C (Figure S2 in the SI) for both solvents used. This is indicative of a clear transition from the amorphous state to a crystalline phase above a particular substrate temperature.

Lamelas and Reid suggested that a variety of routes may exist in the growth of orthorhombic SnO_2.[16] In their work, it was proposed that the formation of metastable tetragonal SnO_2 in the precursor and its subsequent disruption may stimulate nucleation of the orthorhombic phase. In this work, an analogous mechanism may be assumed. First, acetone has a lower boiling point (56−57 °C) than that of methanol (64.7 °C). Differential scanning calorimetry (DSC) experiments (Figure S3 in the SI) indicate that the formation of tin oxide occurs at approximately 210 °C when acetone is used, whereas

DOI: 10.1021/acsami.5b02251
ACS Appl. Mater. Interfaces 2015, 7, 12074−12079

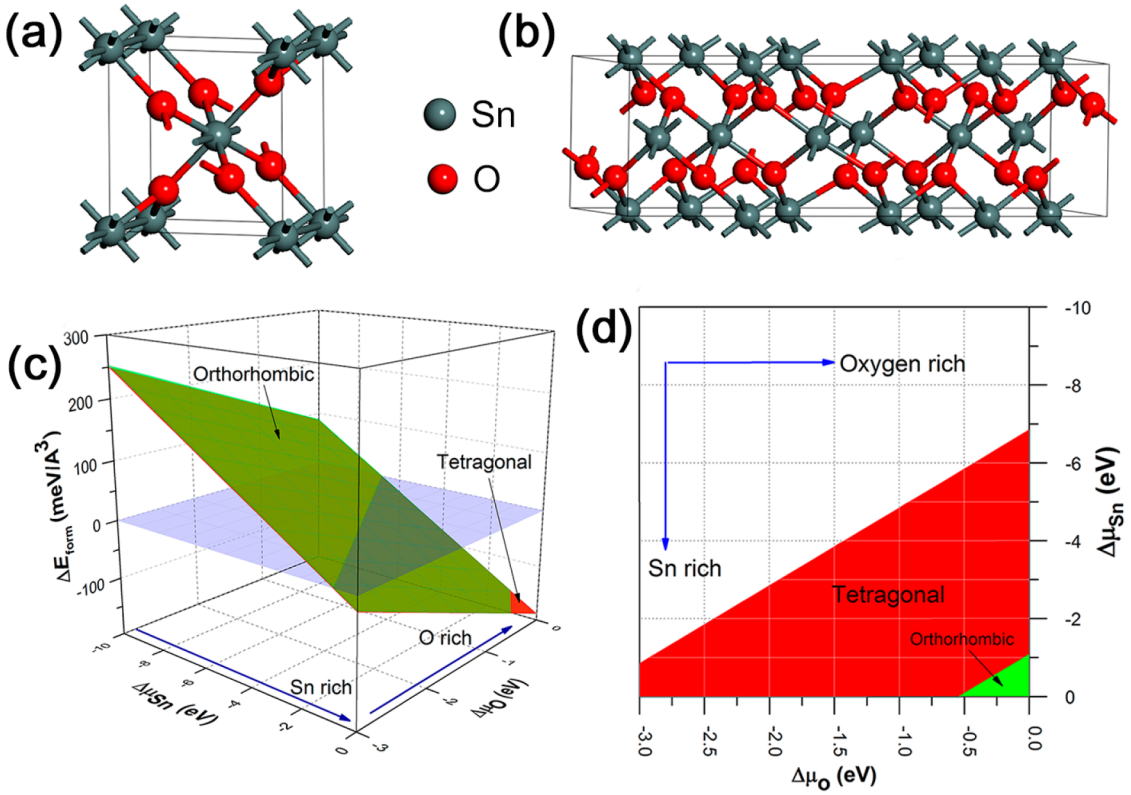

Figure 2. Unit cell structures of SnO_2 phases: (a) tetragonal; (b) orthorhombic. DFT-calculated change in the free energy accompanying the formation of SnO_2 phases: (c) 3D diagram and (d) projected 2D diagram onto the chemical potential surface. Negative values of ΔE_{form} (space below the blue horizontal surface) are required for the spontaneous (thermodynamically driven) formation of SnO_2.

a temperature higher than 250 °C is required for the reaction involving methanol. This is indicative of a tendency for acetone to release oxygen more readily than methanol.

From a morphological point of view, the oxygen atom of the acetone molecule is only bound to carbon through a C═O double bond, whereas the oxygen of the methanol molecule is bound to carbon and hydrogen, forming a C−O−H configuration. Because the nature of the bonds involving oxygen is different between the two solvents, it is not possible to define their relative reactivity by considering the molecular geometry only. Therefore, an additional parameter, ΔE_{red}, was introduced in order to compare the chemical reactivity of the oxygen atoms in methanol and acetone molecules. The oxygen released from the solvent molecule is then assumed to react with the decomposed $SnCl_2{\cdot}2H_2O$ precursor molecules to eventually form metastable tetragonal SnO_2 radicals. By such a mechanism, it is conjectured that the acetone assisting in the formation of metastable tetragonal SnO_2 acts as an intermediate precursor, eventually providing nucleation of orthorhombic crystallites.

Figure 2 shows the DFT-calculated change in free energy accompanying formation of the different SnO_2 phases. For the majority of the chemical potential space, where the formation of SnO_2 phases is thermodynamically driven (i.e., negative ΔE_{form} values), the formation of tetragonal SnO_2 is energetically more favorable. Orthorhombic SnO_2 is stable over only a small portion of the chemical potential space, as indicated in the right-hand bottom corner of Figure 2d, under tin- and oxygen-rich conditions. Because the same tin precursor was used for both methanol and acetone, the oxygen chemical potential is the only controlling variable, suggesting that the formation of orthorhombic SnO_2 requires more reactive oxygen species in the solution. In addition, the calculated reduction energies of methanol (ΔE_{red} = −1.366 eV) and acetone (ΔE_{red} = −1.754 eV) confirm that acetone would supply oxygen more readily for the oxidation of tin to SnO_2. This may support the higher growth rate of the orthorhombic phase compared to that of the tetragonal counterpart (Figure S1 in the SI). The use of acetone thus drives the thermodynamic state of the solution to the right-hand side corner of the oxygen chemical potential space, where the formation of orthorhombic SnO_2 is thermodynamically favored. Our findings suggest that the reduction potential of the solvent may be a key parameter influencing the final crystal structure of SnO_2, which implies that rational design approaches may allow control of the physical and electronic properties of a solid grown by solution-based synthesis.

To study the electrical properties, Hall measurements were carried out on SnO_2 films grown onto insulating glass substrates. All films exhibited n-type conductivity, and the measurement results are indicated in Figure 3, while the parameters are listed in Table 1. It is worth noting that the carrier concentrations in the tetragonal films do not vary much with respect to the substrate temperature at which they were grown, ranging between 10^{14} and 10^{16} cm^{-3}. The Hall mobility values are quite high, ranging approximately between 20 and 60 cm^2/(V s). The orthorhombic films, on the other hand, begin to exhibit high electron concentrations at growth temperatures above 350 °C, up to 10^{19}−10^{21} cm^{-3}, with relatively low Hall mobility values of approximately 0.1−1 cm^2/(V s). Such values are typical of transparent conductive oxides often used as

DOI: 10.1021/acsami.5b02251
ACS Appl. Mater. Interfaces 2015, 7, 12074−12079

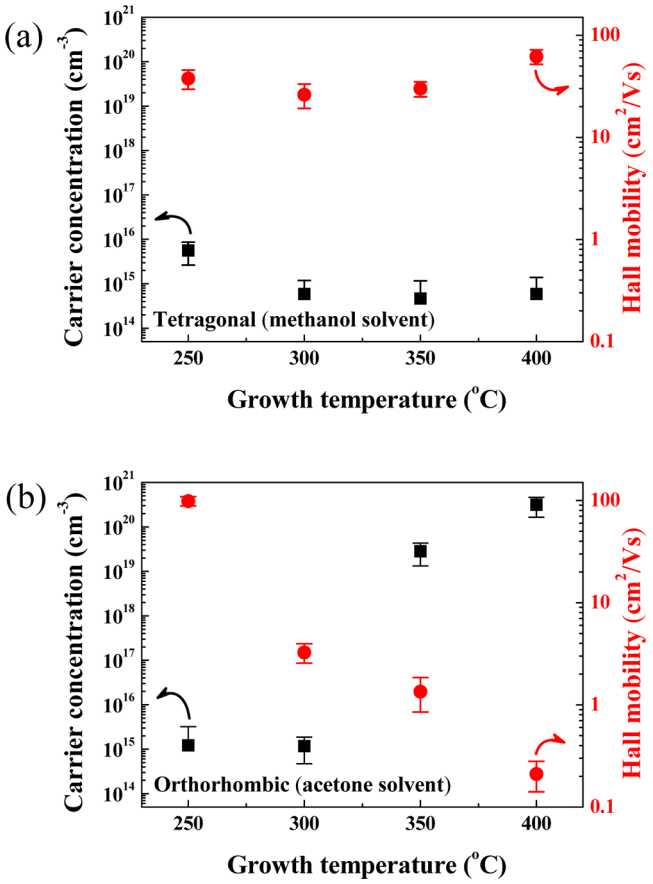

Figure 3. Hall measurement results of SnO_2 films grown using (a) methanol and (b) acetone solvents. Three samples were prepared and analyzed for each growth temperature.

transparent electrodes, with resistivity values of 10^{-4}–10^{-3} Ω cm.

The refractive indices were measured by spectroscopic ellipsometry. Figure S4 in the SI shows the refractive index with respect to the radiation wavelength for tetragonal and orthorhombic SnO_2 films grown at 400 °C. The refractive index of the tetragonal film is higher over the entire range of the visible spectrum, implying the formation of a denser structure.

The optical band-gap values were also compared for each film grown at 400 °C, as illustrated in Figure S5 in the SI. The band gap of the tetragonal SnO_2 is approximately 4.05 eV, while that of the orthorhombic SnO_2 is about 4.14 eV. The larger band gap of the orthorhombic film may be interpreted by the Burstein–Moss blue shift of the absorption spectrum, owing to the relatively abundant carrier concentration.[30,31] It is usually reported that, at carrier concentrations exceeding 10^{19} cm^{-3}, the Fermi energy level is positioned above the conduction band minimum, and the optical absorptive transitions occur from the valence band to the states above the Fermi level. Figure S6 in the SI shows the optical transmittance curve, measured using a UV–vis spectrophotometer. The transmittance of the SnO_2 film grown using the acetone solvent is larger over most of the visible range, which is in good agreement with the optical band-gap observations.

The XPS spectra of the O 1s electrons are illustrated in Figure S7 in the SI for the tetragonal and orthorhombic SnO_2 films grown at 400 °C. To eliminate any possible surface contamination, the XPS spectra were collected after sputtering the surface with neon ions at 500 eV, while preventing the preferential sputtering of light elements. In order to differentiate the detailed oxygen states, the O 1s spectra were carefully deconvoluted into two peaks (O1 and O2) using Gaussian fitting along with subtraction of the Shirley-type background.[32] The low binding energy peak (O1) at approximately 530.7 eV is related to the O^{2-} ions in metal oxides, indicating the presence of Sn–O bonds.[31] On the other hand, the higher binding energy peak (O2) near 531.5 eV is associated with O^{2-} ions in the proximity of oxygen-deficient regions.[33] The relative ratio of the O2 peak ($O2/O_{total}$) indicates that the orthorhombic SnO_2 (0.212) may contain a larger concentration of vacant oxygen sites than the tetragonal phase (0.125).

The electronic band structures of the tetragonal and orthorhombic SnO_2 films were studied using XANES spectroscopy. A comparison of the Sn $M_{4,5}$-edge XANES spectra is given in Figure 4. The Sn $M_{4,5}$-edge spectra show electron

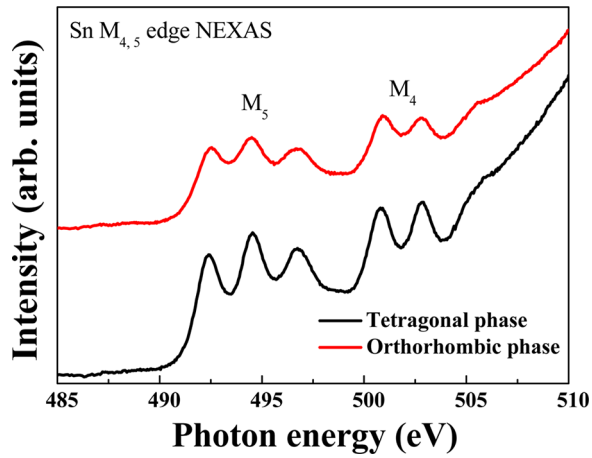

Figure 4. Sn $M_{4,5}$-edge XANES spectra of tetragonal and orthorhombic SnO_2 films grown at 400 °C.

transitions from the Sn 3d core level to unoccupied electronic states above the Fermi level, where M_4 and M_5 correspond to spin–orbit splits into $3d_{3/2}$ and $3d_{5/2}$ levels, respectively.[14] It is clearly observed that the detailed peak splitting and peak ratio in the M_4 and M_5 edges are different between the orthorhombic and tetragonal phases, and the latter exhibits more significant

Table 1. Hall Measurement Results of SnO_2 Films Grown Using Methanol and Acetone Solvents

	tetragonal structure with methanol solvent			orthorhombic structure with acetone solvent		
growth temp (°C)	carrier concn (cm^{-3})	Hall mobility [cm^2/(V s)]	resistivity (Ω cm)	carrier concn (cm^{-3})	Hall mobility [cm^2/(V s)]	resistivity (Ω cm)
250	5.63×10^{15}	37.6	2.64×10^2	1.22×10^{15}	98.6	9.43×10^2
300	5.89×10^{14}	26.2	1.17×10^3	1.17×10^{15}	3.26	1.22×10^4
350	4.68×10^{14}	30	1.04×10^2	2.83×10^{19}	1.35	1.49×10^{-1}
400	5.90×10^{14}	61.8	6.89×10^2	3.15×10^{20}	0.21	1.18×10^{-3}

DOI: 10.1021/acsami.5b02251
ACS Appl. Mater. Interfaces 2015, 7, 12074–12079

peak-to-valley ratios, which is in agreement with previous reports.[14]

TFT devices were fabricated to examine the electrical behavior of tetragonal and orthorhombic SnO_2 films grown at 400 °C. As shown in Figure 5, the device incorporating

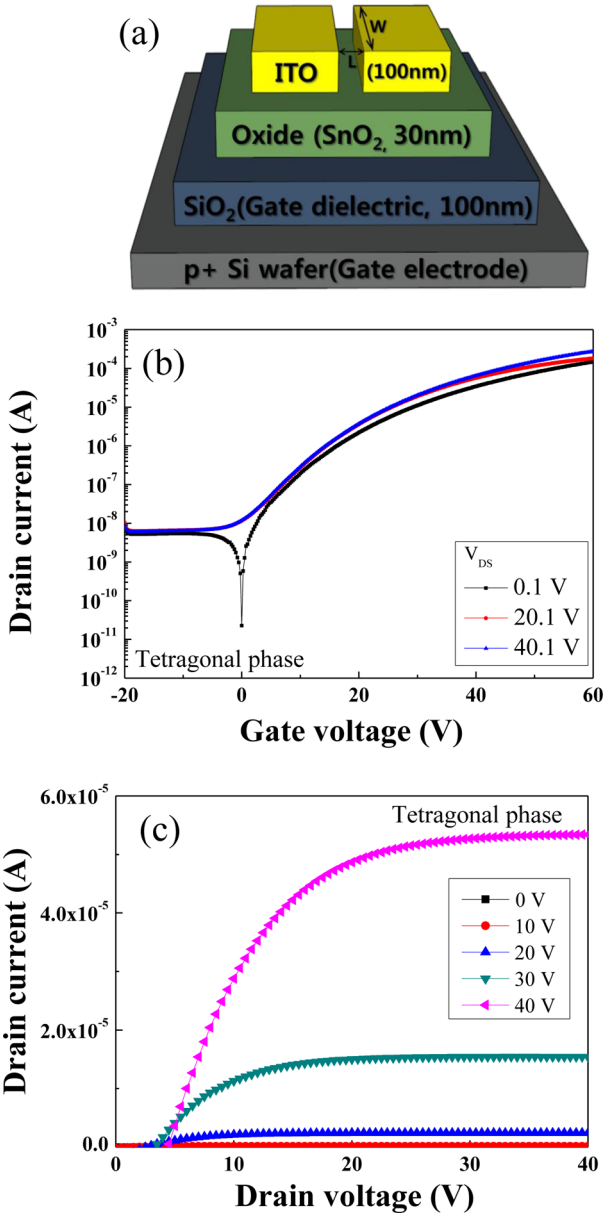

Figure 5. (a) Schematic illustration of the SnO_2 TFT. (b) I_d–V_g characteristics and (c) output curves of a representative TFT device incorporating tetragonal SnO_2 deposited at 400 °C as the active layer.

tetragonal SnO_2 as the active layer exhibits n-type semiconducting behavior, where the drain current (I_d) can be modulated by the applied gate voltage (V_g), hence allowing the realization of a switching element. Saturation mobility values of 3.38 ± 0.4 $cm^2/(V\ s)$ could be extracted from the I_d–V_g curves shown in Figure 5b. Here, the threshold voltages are approximately 4.01 ± 0.1 V with on-to-off current ratios of 10^4. Also, a clear saturation behavior is observed in the output curve in Figure 5b, thus illustrating the semiconducting properties of tetragonal SnO_2. On the other hand, TFT devices incorporating orthorhombic SnO_2 did not show the above characteristics, and the drain current could not be controlled using the gate voltage. Only a relatively large current flowed regardless of the applied gate voltage. This is due to the excessive amount of free electron carriers within the orthorhombic film, which makes it difficult to deplete the channel region of the TFT device. Such a conductive nature of orthorhombic SnO_2 is thus appropriate for transparent electrode applications, with ITO with being one of the most common materials used at present.

CONCLUSION

In the present work, SnO_2 films were grown by Mist-CVD. It was found that the microstructure of the resulting SnO_2 depends greatly on the type of solvent used. Methanol- or acetone-based solutions lead to the formation of tetragonal and orthorhombic phases, respectively. The DFT-calculated reduction energies of methanol and acetone molecules suggest that the acetone molecules are more likely to release free oxygen radicals than methanol molecules, thereby generating higher oxygen density in the precursor solution. The latter is found to be thermodynamically more favorable for the formation of orthorhombic SnO_2. Orthorhombic SnO_2 grown at temperatures above 350 °C exhibits free-electron concentrations larger by several orders of magnitude compared to those of tetragonal SnO_2. Typical n-type semiconducting characteristics were observed in TFTs using tetragonal SnO_2, while devices incorporating orthorhombic SnO_2 exhibited metal-like behavior. The combination of DFT calculations to estimate the reduction energy of specific solvents and their influence on the final crystal structure and properties of SnO_2 films is anticipated to be applicable to other materials, providing ways to achieve the controlled design of functional materials. It will then be possible to synthesize materials with specific physical/electronic properties using simple growth methods under ambient conditions.

ASSOCIATED CONTENT

Supporting Information

Growth rates of the SnO_2 thin films deposited at different temperatures using methanol and acetone solvents (Figure S1), AFM images of the SnO_2 thin films deposited at different temperatures using (a) methanol and (b) acetone solvents (Figure S2), DSC results of tin oxide formation using a tin(II) chloride dehydrate solution with (a) methanol and (b) acetone solvents (Figure S3), refractive index of the tetragonal and orthorhombic SnO_2 films, each deposited using methanol and acetone solvents, respectively (Figure S4), plot of $(\alpha h\nu)^2$ versus photon energy ($h\nu$) of SnO_2 thin films deposited using different solvents at 400 °C (Figure S5), UV–vis transmittance spectra of SnO_2 thin films deposited at different temperatures using different solvents (Figure S6), XPS O 1s spectra of SnO_2 films grown at 400 °C using (a) methanol and (b) acetone solvents (Figure S7), and the thermodynamic stability of SnO_2 phases. The Supporting Information is available free of charge on the ACS Publications website at DOI: 10.1021/acsami.5b02251.

AUTHOR INFORMATION

Corresponding Authors

*E-mail: kimhy@cnu.ac.kr.
*E-mail: khs3297@cnu.ac.kr.
*E-mail: jsparklime@hanyang.ac.kr.

DOI: 10.1021/acsami.5b02251
ACS Appl. Mater. Interfaces 2015, 7, 12074–12079

Author Contributions

‡J.-Y.B. and J.P. (jozeph.park@gmail.com) contributed equally to this work. The manuscript was written through contributions of all authors. All authors have given approval to the final version of the manuscript.

Notes

The authors declare no competing financial interest.

■ ACKNOWLEDGMENTS

This work was mainly supported by the Global Frontier Program through the Global Frontier Hybrid Interface Materials (GFHIM) of the National Research Foundation of Korea (NRF) funded by the Ministry of Science, ICT & Future Planning (2013M3A6B1078870), and partially by Industry technology R&D program of MOTIE/KEIT (Grant No. 10051080). Also, this work was partially supported by research fund of Chungnam National University. In particular, the authors thank to Dr. Minseok Choi (Korea Institute of Material Science) for discussing ab initio calculation and electronic structures on Mist-CVD SnO_2 works.

■ REFERENCES

(1) Snaith, H. J.; Ducati, C. SnO_2-Based Dye-Sensitized Hybrid Solar Cells Exhibiting Near Unity Absorbed Photon-to-Electron Conversion Efficiency. *Nano Lett.* **2010**, *10* (4), 1259−1265.

(2) Vilà, A.; Gomez, A.; Portilla, L.; Morante, J. R. Influence of In and Ga Additives onto SnO_2 Inkjet-Printed Semiconductor. *Thin Solid Films* **2014**, *553*, 118−122.

(3) Song, H.; Lee, K. H.; Jeong, H.; Um, S. H.; Han, G. S.; Jung, H. S.; Jung, G. Y. A Simple Self-Assembly Route to Single Crystalline SnO_2 Nanorod Growth by Oriented Attachment for Dye Sensitized Solar Cells. *Nanoscale* **2013**, *5*, 1188−1194.

(4) Lee, S. C.; Lee, J. H.; Oh, T. S.; Kim, Y. H. Fabrication of Tin Oxide Film by Sol−Gel Method for Photovoltaic Solar Cell System. *Sol. Energy Mater. Sol. Cells* **2003**, *75*, 481−487.

(5) Suehle, J. S.; Cavicchi, R. E.; Gaitan, M.; Semancik, S. Tin Oxide Gas Sensor Fabricated using CMOS Micro-Hotplates and In-situ Processing. *IEEE Electron Device Lett.* **1993**, *14* (3), 118−120.

(6) Watson, J.; Ihokura, K.; Coles, G. S. V. The Tin Dioxide Gas Sensor. *Meas. Sci. Technol.* **1993**, *4*, 711−719.

(7) Nayral, C.; Ould-Ely, T.; Maisonnat, A.; Chaudret, B.; Fau, P.; Lescouzeres, L.; Peyre-Lavigne, A. A Novel Mechanism for the Synthesis of Tin/Tin Oxide Nanoparticles of Low Size Dispersion and of Nanostructured SnO_2 for the Sensitive Layers of Gas Sensors. *Adv. Mater.* **1999**, *11* (1), 61−63.

(8) Johari, A.; Bhatnagar, M. C.; Rana, V. Low Temperature Tin Oxide (SnO_2) Nanowire Gas Sensor. *Proc. SPIE—Int. Soc. Opt. Eng.* **2012**, *8549*, 854915.

(9) Dattoli, E. N.; Davydov, A. V.; Benkstein, K. D. Tin Oxide Nanowire Sensor with Integrated Temperature and Gate Control for Multi-Gas Recognition. *Nanoscale* **2012**, *4*, 1760−1769.

(10) Mubeen, S.; Lai, M.; Zhang, T.; Lim, J. H.; Mulchandani, A.; Deshusses, M. A.; Myung, N. V. Hybrid Tin Oxide−SWNT Nanostructures Based Gas Sensor. *Electrochim. Acta* **2013**, *92*, 484−490.

(11) Dai, Z. R.; Gole, J. L.; Stout, J. D.; Wang, Z. L. Tin Oxide Nanowires, Nanoribbons, and Nanotubes. *J. Phys. Chem. B* **2002**, *106*, 1274−1279.

(12) Suito, K.; Kawai, N.; Masuda, Y. High Pressure Synthesis of Orthorhombic SnO_2. *Mater. Res. Bull.* **1975**, *10*, 677−680.

(13) Liu, L. G. A Fluorite Isotype of SnO_2 and a New Modification of TiO_2: Implications for the Earth's Lower Mantle. *Science* **1978**, *199* (4327), 422−425.

(14) Chen, Z.; Lai, J. K. L.; Shek, C. H. Facile Strategy and Mechanism for Orthorhombic SnO_2 Thin Films. *Appl. Phys. Lett.* **2006**, *89*, 231902.

(15) Kaplan, L.; Ben-Shalom, A.; Boxman, R. L.; Goldsmith, S.; Rosenberg, U.; Nathan, M. Annealing and Sb-doping of Sn−O films produced by filtered vacuum arc deposition: structure and electro-optical properties. *Thin Solid Films* **1994**, *253*, 1−8.

(16) Lamelas, F. J.; Reid, S. A. Thin-Film Synthesis of the Orthorhombic Phase of SnO_2. *Phys. Rev. B: Condens. Matter Mater. Phys.* **1999**, *60* (13), 9347.

(17) Chang, J. F.; Sun, B. Q.; Breiby, D. W.; Nielsen, M. M.; Sölling, T. I.; Giles, M.; McCulloch, I.; Sirringhaus, H. Enhanced Mobility of Poly(3-hexylthiophene) Transistors by Spin-Coating from High-Boiling-Point Solvents. *Chem. Mater.* **2004**, *16*, 4772.

(18) Edusi, C.; Sankar, G.; Parkin, I. P. The Effect of Solvent on the Phase of Titanium Dioxide Deposited by Aerosol-assisted CVD. *Chem. Vap. Deposition* **2012**, *18*, 126−132.

(19) Okuno, T.; Oshima, T.; Lee, S. D.; Fujita, S. Growth of SnO_2 Crystalline Thin Films by Mist Chemical Vapor Deposition Method. *Phys. Status Solidi C* **2011**, *8* (2), 540−542.

(20) Jeon, H. J.; Lee, S. G.; Kim, H.; Park, J. S. Enhanced Mobility of Li-Doped ZnO Thin Film Transistors Fabricated by Mist Chemical Vapor Deposition. *Appl. Surf. Sci.* **2014**, *301*, 358−362.

(21) Kresse, G.; Furthmuller, J. Efficiency of Ab-Initio Total Energy Calculations for Metals and Semiconductors using a Plane-Wave Basis Set. *Comput. Mater. Sci.* **1996**, *6*, 15−50.

(22) Singh, A. K.; Janotti, A.; Scheffler, M.; Van de Walle, C. G. Sources of Electrical Conductivity in SnO_2. *Phys. Rev. Lett.* **2008**, *101*, 055502.

(23) Ágoston, P.; Albe, K.; Nieminen, R. M.; Puska, M. J. Intrinsic n-Type Behavior in Transparent Conducting Oxides: A Comparative Hybrid-Functional Study of In_2O_3, SnO_2, and ZnO. *Phys. Rev. Lett.* **2009**, *103*, 245501.

(24) Blöchl, P. E. Projector Augmented-Wave Method. *Phys. Rev. B: Condens. Matter Mater. Phys.* **1994**, *50*, 17953.

(25) Perdew, J. P.; Ernzerhof, M.; Burke, K. Rationale for Mixing Exact Exchange with Density Functional Approximations. *J. Chem. Phys.* **1996**, *105*, 9982−9985.

(26) Heyd, J.; Scuseria, G. E.; Ernzerhof, M. Erratum: "Hybrid Functionals Based on a Screened Coulomb Potential" [J. Chem. Phys. 118, 8207 (2003)]. *J. Chem. Phys.* **2006**, *124*, 219906.

(27) Yang, F.; Kundu, S.; Vidal, A. B.; Graciani, J.; Ramírez, P. J.; Senanayake, S. D.; Stacchiola, D.; Evans, J.; Liu, P.; Sanz, J. F.; Rodriguez, J. A. Determining the Behavior of RuOx Nanoparticles in Mixed-Metal Oxides: Structural and Catalytic Properties of RuO_2/TiO_2(110) Surfaces. *Angew. Chem., Int. Ed.* **2011**, *50*, 10198−10202.

(28) Becke, A. D. Density-Functional Thermochemistry. III. The Role of Exact Exchange. *J. Chem. Phys.* **1993**, *98*, 5648−5652.

(29) Stephens, P. J.; Devlin, F. J.; Chabalowski, C. F.; Frisch, M. J. Ab Initio Calculation of Vibrational Absorption and Circular Dichroism Spectra Using Density Functional Force Fields. *J. Phys. Chem.* **1994**, *98*, 11623−11627.

(30) Ye, J. D.; Gu, S. L.; Zhu, S. M.; Liu, S. M.; Zheng, Y. D.; Zhang, R.; Shi, Y.; Yu, H. Q.; Ye, Y. D. Gallium Doping Dependence of Single-Crystal n-type ZnO Grown by Metal Organic Chemical Vapor Deposition. *J. Cryst. Growth* **2005**, *283*, 279−285.

(31) Kim, C. E.; Moon, P.; Kim, S.; Myoung, J. M.; Jang, H. W.; Bang, J.; Yun, I. Effect of Carrier Concentration on Optical Bandgap Shift in ZnO:Ga Thin Films. *Thin Solid Films* **2010**, *518*, 6304−6307.

(32) Ahn, B. D.; Lim, J. H.; Cho, M. H.; Park, J. S.; Chung, K. B. Thin-Film Transistor Behavior and the Associated Physical Origin of Water-Annealed In−Ga−Zn Oxide Semiconductor. *J. Phys. D: Appl. Phys.* **2012**, *45*, 415307.

(33) Ke, C.; Zhu, W.; Pan, J. S.; Yang, Z. Annealing Temperature Dependent Oxygen Vacancy Behavior in SnO_2 Thin Films Fabricated by Pulsed Laser Deposition. *Curr. Appl. Phys.* **2011**, *11*, S306.

DOI: 10.1021/acsami.5b02251
ACS Appl. Mater. Interfaces 2015, 7, 12074−12079